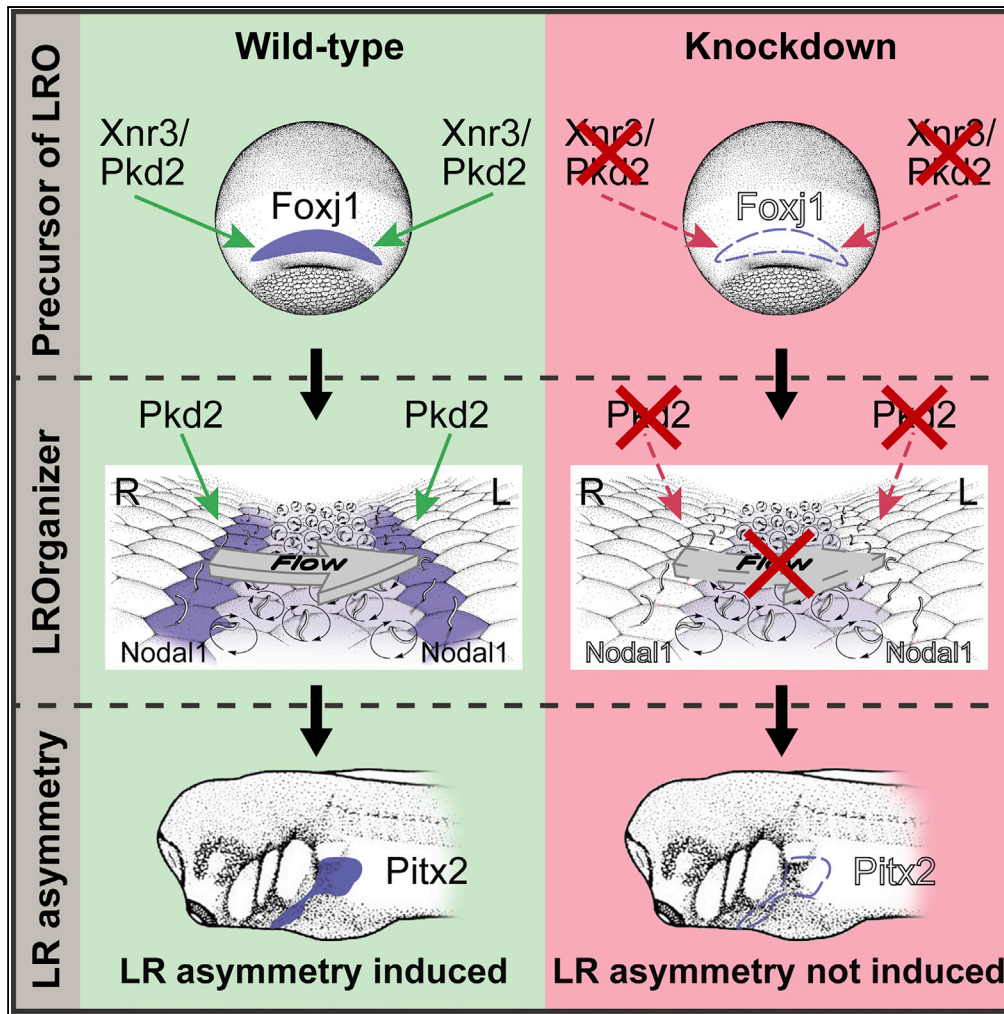


Article

An Early Function of Polycystin-2 for Left-Right Organizer Induction in *Xenopus*



Philipp Vick,
Jennifer Kreis,
Isabelle
Schneider, ..., Tina
Beyer, Axel
Schweickert,
Martin Blum

philipp.vick@uni-hohenheim.de

HIGHLIGHTS

Loss of Polycystin-2 in *Xenopus* results in LR asymmetry defects upstream of leftward flow

LR defects are caused by lack of LR organizer induction

Polycystin-2 is required upstream of *foxj1* for specification of superficial mesoderm

Polycystin-2 and *Xnr3* synergistically induce *foxj1* in the superficial mesoderm

Vick et al., iScience 2, 76–85
April 27, 2018 © 2018 The
Author(s).
[https://doi.org/10.1016/
j.isci.2018.03.011](https://doi.org/10.1016/j.isci.2018.03.011)



Article

An Early Function of Polycystin-2 for Left-Right Organizer Induction in *Xenopus*

Philipp Vick,^{1,6,*} Jennifer Kreis,¹ Isabelle Schneider,^{1,2} Melanie Tingler,¹ Maike Getwan,^{1,3} Thomas Thumberger,^{1,4} Tina Beyer,^{1,5} Axel Schweickert,¹ and Martin Blum¹

SUMMARY

Nodal signaling controls asymmetric organ placement during vertebrate embryogenesis. Nodal is induced by a leftward fluid flow at the ciliated left-right organizer (LRO). The mechanism of flow sensing, however, has remained elusive. *pkd2* encodes the calcium channel Polycystin-2, which is required for kidney development and laterality, and may act in flow perception. Here, we have studied the role of Polycystin-2 in *Xenopus* and show that *pkd2* is indispensable for left-right (LR) asymmetry. Knockdown of *pkd2* prevented left-asymmetric nodal cascade induction in the lateral plate mesoderm. Defects were due to failure of LRO specification, morphogenesis, and, consequently, absence of leftward flow. Polycystin-2 synergizes with the unconventional nodal-type signaling molecule *Xnr3* to induce the LRO precursor tissue before gastrulation, upstream of symmetry breakage. Our data uncover an unknown function of *pkd2* in LR axis formation, which we propose represents an ancient role of Polycystin-2 during LRO induction in lower vertebrates.

INTRODUCTION

Asymmetries along the left-right (LR) body axis are a common feature of most animals. Vertebrates, for example, show asymmetric arrangements of most visceral organs (Grimes and Burdine, 2017). In all deuterostomes examined, as well as in several protostomes, asymmetries are induced by unilateral activation of the Nodal signaling cascade, consisting of *nodal*, *lefty*, and *pitx2*, before onset of asymmetric organogenesis (Namigai et al., 2014; Shiratori and Hamada, 2014). How the Nodal cascade is activated unilaterally is a matter of intense research. The most common symmetry-breaking mechanism in vertebrates is a transient extracellular leftward fluid flow at the archenteron of gastrula/neurula embryos (Blum et al., 2009). Although this flow lost in birds, it is absolutely required for symmetry breakage in rabbit, mouse, frog, and fish (Essner et al., 2005; Nonaka et al., 1998; Schweickert et al., 2007). Flow is generated at the left-right organizer (LRO), a transient ciliated epithelium. Owing to the clockwise rotation of monocilia and their posterior tilting, they generate a leftward flow of extracellular fluids (Blum et al., 2014b; Yoshiba and Hamada, 2014). Putative LROs have been pinpointed in further vertebrates (axolotl, additional frog species, sturgeon), the ancient chordate amphioxus, and the sea urchin *Paracentrotus* (Blum et al., 2009; Sáenz-Ponce et al., 2011; Tisler et al., 2016).

How flow is sensed on the left side of the LRO and how it activates the Nodal cascade in the lateral plate mesoderm (LPM) is still largely unknown. The Nodal inhibitor *Dand5* is one decisive factor in chordates. *dand5* and *nodal* are expressed bilaterally on both sides of the LRO, just before flow becomes established. As a result of flow, *dand5* becomes down-regulated on the left (Schweickert et al., 2010; Shinohara et al., 2012). In *Xenopus*, knockdown of *dand5* rescues flow-deficient embryos, establishing *dand5* mRNA asymmetry as the first detectable molecular feature of LR asymmetry. How this inhibition is realized at the cellular level is not known. One mechanism that has been proposed is a calcium-dependent down-regulation of *dand5* during flow (Yoshiba et al., 2012). Left-sided calcium fluxes during flow stages have been described and implicated in flow sensing, but the molecular consequences have remained elusive (Sarmah et al., 2005; Yuan et al., 2015). According to the two-cilia model of symmetry breakage, motile cilia at the center of the LRO create a leftward flow that bends immotile mechanosensory cilia at the left margin. This bending results in left-sided calcium fluxes, which supposedly activate downstream calcium-dependent events that break the bilateral symmetry (McGrath et al., 2003; Tabin and Vogan, 2003). Genetic experiments in the mouse have unequivocally demonstrated that the calcium channel Polycystin-2 is specifically required in lateral cells of the mouse LRO to break symmetry (Yoshiba et al., 2012).

We and others have previously shown that *pkd2*, the gene encoding Polycystin-2, is necessary for kidney and LR development in mouse and for kidney development in *Xenopus*, as it is in other vertebrates (Futel

¹Institute of Zoology, University of Hohenheim, 70599 Stuttgart, Germany

²Present address: Molecular Cardiology, University Hospital Ulm, 89081 Ulm, Germany

³Present address: Department of Medicine, Renal Division, Medical Center-University of Freiburg, Faculty of Medicine, University of Freiburg, 79106 Freiburg, Germany

⁴Present address: Center for Organismal Studies, Heidelberg University, 69120 Heidelberg, Germany

⁵Present address: Institute for Ophthalmic Research, Center for Ophthalmology, University of Tübingen, 72076 Tübingen, Germany

⁶Lead Contact

*Correspondence: philipp.vick@uni-hohenheim.de
<https://doi.org/10.1016/j.isci.2018.03.011>



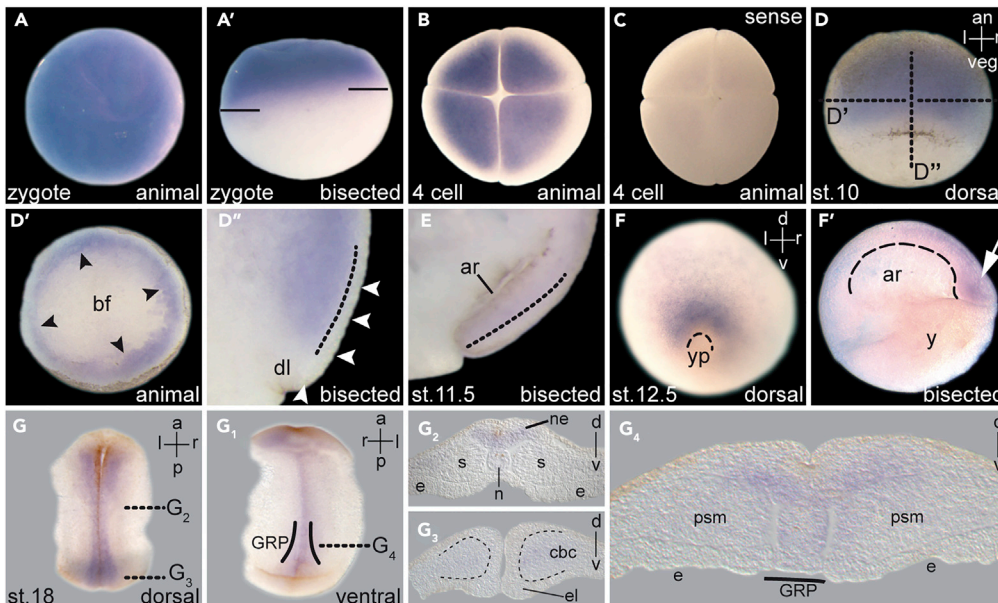


Figure 1. Expression of *pkd2* mRNA during *Xenopus* Embryogenesis

(A–C) Maternally deposited mRNA localized to the animal hemisphere of the zygote (A, A') and four-cell stage embryos (B). Note animal-vegetal shift of expression as indicated in the zygote. (C) Lack of a specific signal in specimen hybridized with a sense probe.

(D–F) *pkd2* transcripts in deep mesodermal layers of the early gastrula (D, D', D''; black arrowheads; plane of section indicated in D by dotted line), in dorsal notochordal mesoderm at mid gastrula (E), and in tail organizer (white arrow) and posterior notochord at late gastrula stages (F, F'). Please note the lack of transcripts in the dorsal lip and the SM (white arrowheads). Border of inner and outer layer of marginal zone indicated by dotted line. Yolk plug and archenteron roof indicated by dashed lines.

(G) Deep neuroectodermal, tail organizer, and posterior notochordal expression at neurula stages; no expression of GRP detected (G₄).

a, anterior; an, animal; ar, archenteron; bf, blastocoel floor; cbc, circumblastoporal collar; dl, dorsal lip; e, endoderm; el, epithelial layer (of cbc); l, left; n, notochord; ne, neuroectoderm; psm, presomitic mesoderm; r, right; s, somites; v, ventral; veg, vegetal; yp, yolk plug.

See also Figure S1.

et al., 2015; Pennekamp et al., 2002; Sullivan-Brown et al., 2008; Tran et al., 2010). Here, we revisited the role of Polycystin-2 in LR development in *Xenopus*, in which the sequential steps of laterality development are known in great detail and can be experimentally manipulated in a sided manner. *pkd2* knock-down resulted in failure of Nodal cascade activation, as previously shown for fish and mouse. LRO morphogenesis and function were lost in morphants, as revealed by altered marker gene expression and a lack of ciliation and leftward flow. This phenotype was due to a lack of *pkd2*-dependent induction of the LRO precursor tissue, the superficial mesoderm (SM), during early gastrulation. Polycystin-2 and the FGFR-binding ligand Xnr3 synergize to induce *foxf1* in the SM, establishing an unknown function of Polycystin-2.

RESULTS AND DISCUSSION

pkd2 Is Required for LR Axis Development in *Xenopus*

As a reference point for the functional assessment of *pkd2* during symmetry breakage, we analyzed mRNA expression during embryogenesis. Signals at the animal pole of the zygote and during early cleavage stages represented maternally deposited transcripts (Figures 1A and 1B). Sense probe control specimens lacked staining (Figure 1C; data not shown). During early gastrulation, *pkd2* was restricted to the deep mesoderm, excluding the dorsal lip and the superficial epithelial layer, i.e., the SM, from which the LRO, the gastrocoel roof plate (GRP), develops during gastrulation (Figure 1D; Blum et al., 2014a). Later expression sites included the notochord, trunk organizer, deep neuroectoderm, intermediate mesoderm, and developing pronephric kidney (Figures 1E–1G and S1A–S1E; cf. Tran et al., 2010).

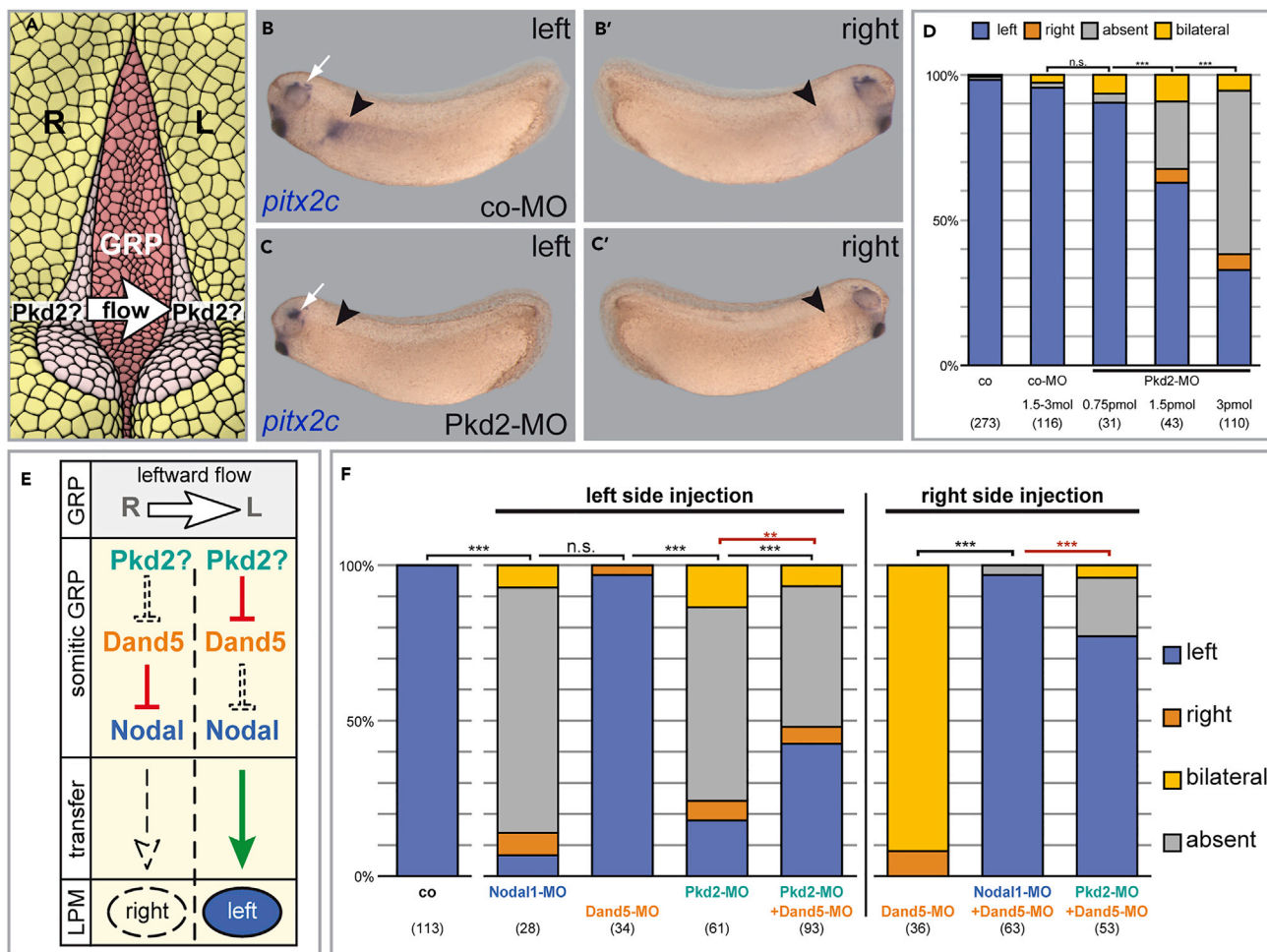


Figure 2. *pkd2* Is Required for LR Asymmetry in *Xenopus*, Independently of *dand5*

(A) Putative sensory function of Polycystin-2 during symmetry breakage downstream of GRP-flow.

(B–D) Dose-dependent loss of left-sided *pitx2c* expression following *Pkd2*-MO targeting to the GRP. Black arrowhead indicates approximate location of present or absent *pitx2c* expression on both sides of the embryo. White arrow highlights expression of *pitx2c* around the eye as proof of working ISH.

(E) Model of hierarchy of the flow sensing module and possible role of *pkd2* on the lateral side of the LRO downstream of flow and upstream of *Dand5*.

(F) Epistatic single and double knockdown experiments, performed on the left or right side, as indicated. Differences in expected and experimental outcome highlighted by red significance. See text for details.

See also Figure S2.

p < 0.01, *p < 0.001 in all Figures.

Numbers in parentheses indicate the number of embryos analyzed for each condition.

Remarkably, zygotic *pkd2* mRNA was not detected in the SM or in the GRP (Figures 1D and 1G), i.e., the early LR-relevant tissues.

In the mouse, Polycystin-2 acts downstream of flow but upstream of flow-dependent *dand5* repression and LPM *Nodal* induction (Yoshida et al., 2012). To test whether this function was conserved in *Xenopus*, we targeted a previously characterized antisense morpholino oligomer (MO) that blocks translation of *pkd2* (*Pkd2*-MO; Tran et al., 2010) to the future GRP (cf. Figure 2A). Morphant embryos lacked induction of the *Nodal* cascade in the left LPM in a dose-dependent manner, in agreement with this notion (Figures 2B–2D). As expected for a flow-sensing function, *pkd2* was required on the left side of the GRP, as revealed by unilateral injections (Figures S2A and S2B; cf. Vick et al., 2009 for left-sided flow knockdown). Knockdown in the LPM itself did not cause LR defects, suggesting that *pkd2* was not relevant for *Nodal*

propagation (Figure S2B). In summary, these results showed that *pkd2* was required for the activation of the Nodal cascade in the left LPM, suggesting a conserved role during flow-dependent symmetry breakage.

Pkd2* Functions Independently of *dand5

Dand5 plays a key role at the interface between flow and Nodal induction (Figure 2E). To test whether *pkd2* acted upstream of *dand5* in the process of flow sensing, we performed combinatory knockdown experiments. When *Pkd2*-MO was injected on the left side of the GRP, embryos failed to induce *pitx2c* in the left LPM, similar to a GRP-specific *nodal1* knockdown. Inhibition of *dand5* alone had no effect, as described (Figure 2F; cf. Schweickert et al., 2010), because flow down-regulates *dand5* as a physiological target. When *Pkd2*-MO and *Dand5*-MO were co-injected, most specimens still did not induce *pitx2c* (Figure 2F). *Dand5* knockdown thus failed to rescue loss of Polycystin-2, as was expected from the sensor function described in mouse (Figure 2E). *Pkd2* therefore could act upstream of *nodal* induction in the LPM. Knockdown of *pkd2* in the LPM, however, did not affect *pitx2* expression (Figure S2B). Alternatively, *pkd2* could be required for *nodal* function at the lateral cells (sensory part) of the GRP. The possibility of sided injections in *Xenopus* afforded the opportunity of investigating this notion on the right side of the GRP, independently of flow. Here, *dand5* knockdown induces right-sided Nodal cascade induction (Figure 2F; cf. Schweickert et al., 2010). Parallel knockdown of *dand5* and *nodal1* at the right GRP margin counteracted this effect, as loss of the Nodal inhibitor *Dand5* can only be effective in the presence of Nodal. Simultaneous targeting of *Dand5*-MO and *Pkd2*-MO to the right GRP margin still prevented right-sided Nodal cascade induction (Figure 2F), suggesting that *pkd2* was required for Nodal function at the GRP or GRP function in general.

Leftward Flow and GRP Morphogenesis Are Compromised in *pkd2* Morphants

The high efficiency of *Pkd2*-MO, comparable with a *nodal1* knockdown in the left GRP, asked for an in-depth analysis of GRP function itself. Leftward flow was analyzed in dorsal explants prepared from flow stage embryos that were injected with control (co-)MO or *Pkd2*-MO as described (Vick et al., 2009). Time-lapse videography of fluorescent beads added to the explants demonstrated that flow was absent at the targeted area in morphants (Figures 3A, 3C, and Video S1), whereas co-MO injected specimens displayed the previously reported directionality and velocity of bead transport (Figures 3B and 3D; cf. Schweickert et al., 2007). This result suggested that GRP function was lost in *pkd2* morphants. A morphological analysis of GRP tissue using immunofluorescence (IF) to highlight cilia and cell boundaries confirmed this notion, as cilia were literally absent (Figures 3E–3G). To gain further insights into the nature of GRP defects, scanning electron microscopy (SEM) was employed. co-MO-injected specimens (Figure S3A; n = 6) displayed on average 88% ciliated GRP cells, whereas this rate dropped to 34% in *pkd2* morphants, and remaining ciliated cells lacked polarization (Figure S3B; n = 5). Individual specimens lacked cilia altogether. Remarkably, non-ciliated morphant cells revealed an increase in cell surface area and thus resembled endodermal cells rather than the small GRP cells (Figure S3B), indicating a potential change of fate. GRP marker genes, such as the tektin isoform *tekt2* as well as the axonemal dynein motor protein *dnah9*, were absent from morphant explants, whereas control samples exhibited wild-type expression patterns (Figures 3H–3K, S3C, and S3D). Importantly, GRP ciliation and gene expression were rescued by co-injection of a full-length *pkd2* mRNA construct that was not targeted by the *Pkd2*-MO (Figures 3G, 3J, and 3K).

To investigate the GRP fate in depth, we analyzed marker genes that highlight the lateral sensory cells, namely, *nodal1* and *dand5*. Both were absent from morphant specimens, in which *Pkd2*-MO was targeted to these cells (Figures 3L, 3M and S3E–S3H). A further SEM analysis revealed that lateral GRP cells were missing completely and that remaining ciliated central GRP cells directly bordered non-ciliated endodermal cells (Figure S3I). In the absence of *nodal1*, the *Dand5*-MO thus remained without effect, providing a stringent explanation for the nearly complete lack of *pitx2c* induction upon *dand5* knockdown in *pkd2* morphants (cf. Figure 2F).

Polycystin-2 is mainly part of a cilia- or endoplasmic reticulum (ER)-located calcium channel complex, which can modulate cellular calcium levels, and itself can be regulated by intracellular calcium (Busch et al., 2017). To test if manipulations of intracellular calcium levels also affected *nodal1* expression, we treated embryos with Thapsigargin (Tg), a well-known antagonist of ER-located SERCA pumps (Thastrup et al., 1990). Embryos treated at early gastrulation showed blastopore closure defects, caused by lack of necessary intracellular calcium waves, as previously reported (Wallingford et al., 2001; data not shown). Treatment from late

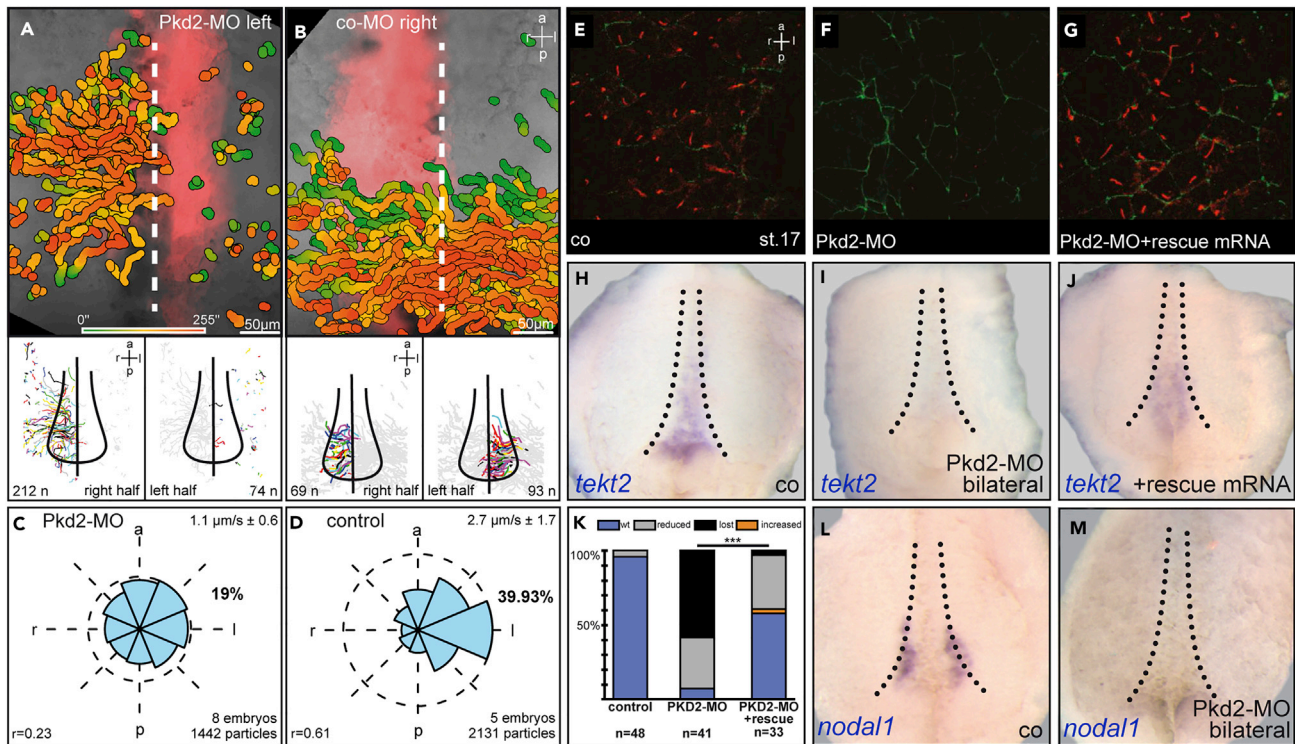


Figure 3. Leftward Flow and GRP Morphogenesis Are Compromised in *pkd2* Morphants

(A–D) Unilateral injection of Pkd2-MO (A) but not co-MO (B) caused disruption of leftward flow at targeted area (red fluorescence: lineage tracer), as revealed by gradient time trail (GTT); see [Transparent Methods](#) section and [Schweickert et al., \(2007\)](#) analysis. Quantification of directionality and velocity of bead transport on morphant (C) and control (D) sides of dorsal explants. Rho (r) represents a value for robustness of directionality of leftward flow. Scale bars represent 50 micrometers.

(E–G) Stage 17 GRP ciliation (E) was lost in *pkd2* morphants (F) and regained in specimens co-injected with *pkd2*-MO and a full-length *pkd2* mRNA. IF with acetylated α -tubulin antibodies (red) and Alexa 488-phalloidin (green) to highlight GRP cilia and cell borders.

(H–K) *tekt2* expression at the GRP of stage 17 dorsal explants (H) was lost in *pkd2* morphants (I) and rescued upon co-injection of a full-length *pkd2* mRNA (J).

(K) Quantification of results.

(L and M) *nodal1* expression in lateral GRP cells (L) was lost in morphants (M).

See also [Figure S3](#) and [Video S1](#)

gastrula stages onward, however, did not affect gastrulation and resulted in reduced or absent *nodal1* expression at neurula stages, i.e., when *nodal1* is initiated in lateral GRP cells before flow occurs ([Figures S3J–S3L](#)). This outcome was supported by another set of experiments. When embryos were treated in the same way with BAPTA-AM, an intracellular calcium chelator, they also showed reduced expression of *nodal1* at neurula stages ([Figures S3M–S3P](#)). These results support the notion that Polycystin-2 is necessary to induce the lateral cell fate of the LRO in *Xenopus*, and this required intracellular calcium changes. Yet, these findings were unexpected, as altered LRO *nodal* expression was not reported from *pkd2*-knockout mice or zebrafish morphants ([Bisgrove et al., 2005](#); [Pennekamp et al., 2002](#)). Mouse embryos treated with Tg, however, showed loss of *nodal1* in the LRO and LPM as well, arguing for conservation of a calcium-dependent induction of lateral LRO fates ([Takao et al., 2013](#)). Taken together, these analyses demonstrated that LR defects in *Pkd2* morphants were caused by impaired GRP morphogenesis and function and, specifically, the absence of lateral LRO cells expressing *nodal1* and *dand5*.

pkd2 Is Required for SM Specification

Next, we asked whether the GRP precursor tissue, the SM, was correctly specified during gastrulation. To that end, we analyzed SM marker genes *xnr3* and *foxf1*. Both genes are known targets of canonical Wnt signaling; *foxf1* is instrumental for SM and GRP function downstream of Wnt signaling ([Glinka et al., 1996](#); [Smith et al., 1995](#); [Stubbs et al., 2008](#); [Walentek et al., 2013](#)). Remarkably, these genes responded differently to *pkd2* knockdown: *xnr3* was slightly upregulated, whereas *foxf1* expression was reduced or absent ([Figures 4A–4F](#)). This effect was specific, as *foxf1* expression was rescued (or even super-induced) upon

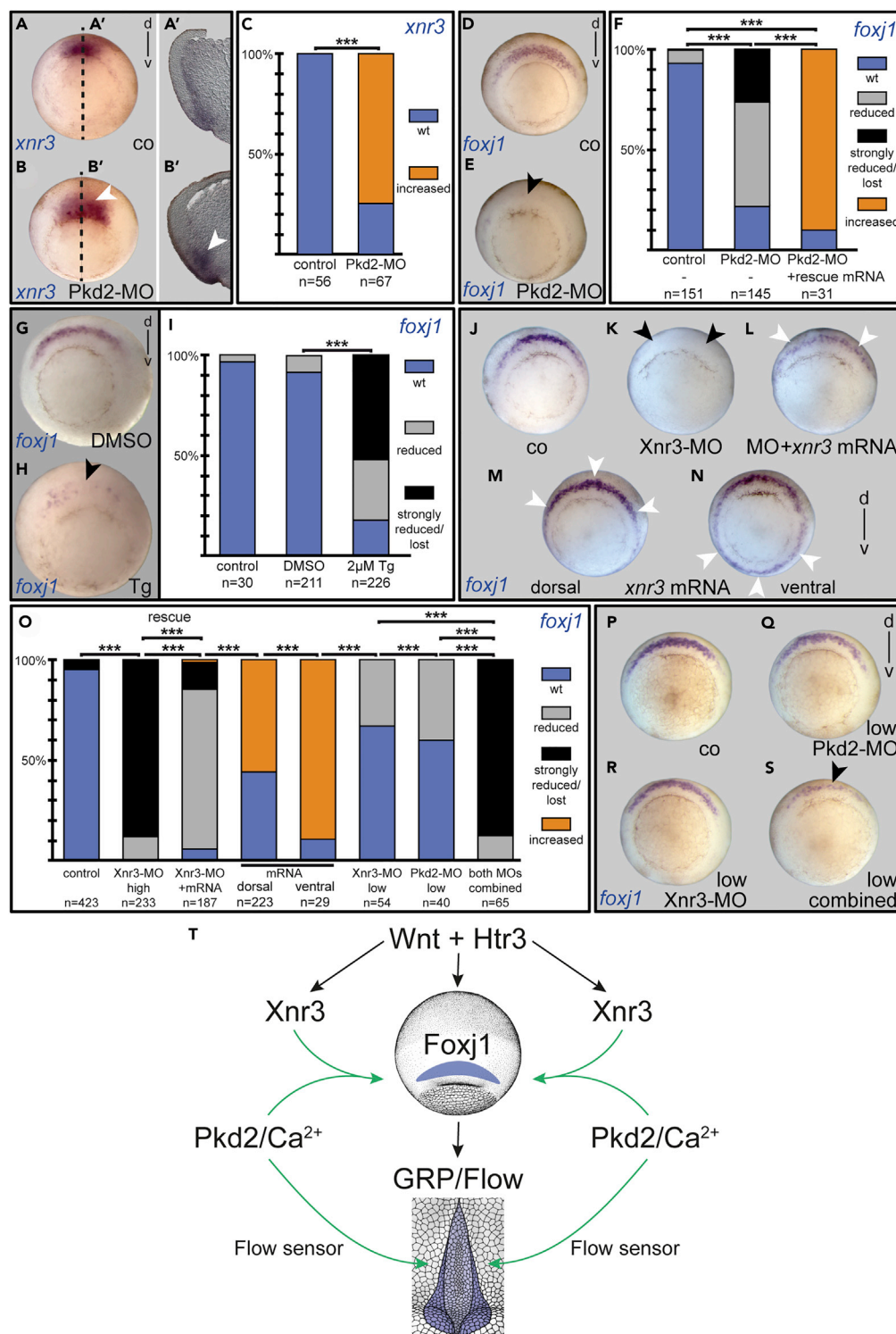


Figure 4. Polycystin-2 and Xnr3 Synergize to Induce the LRO Precursor Tissue of the Superficial Mesoderm
 (A–F) Increased *xnr3* (A–C) and reduced *foxj1* expression (D–F) in stage 10.5 *pkd2* morphants (B and E) as compared with control specimens (A and D). Dotted lines in A and B indicate plane of histological sections shown in A', and B', respectively. Note that *foxj1* expression was rescued upon co-injection of a full-length *pkd2* mRNA (F).
 (G–I) Reduced *foxj1* expression in early gastrula stages (st. 10.5) following Tg treatment (G, DMSO control embryo; H, Tg treated specimen; I, quantification of results).

Figure 4. Continued

(J–S) *xnr3* and *pkd2* synergize SM *foxj1* induction. Loss of *xnr3* resulted in attenuated *foxj1* expression (K and O) compared with control uninjected specimens (J and O), which was highly efficiently rescued by co-injection of full-length *xnr3* mRNA (L and O). Both dorsal (M) and ventral (N) overexpression of *xnr3* mRNA caused an increase of endogenous or induction of ectopic *foxj1*, respectively (M–O). Injections of reduced MO doses of Xnr3-MO (O, R; $2 \times 0.6\text{pmol}$) or Pkd2-MO (O, Q; $2 \times 0.75\text{pmol}$) caused mild reductions of *foxj1* expression. Co-injection of low doses of MOs resulted in strong inhibitory effects (O and S). (T) Schematic depiction of known (black) and proposed (green) interactions required for SM specification. For details refer to main text. Increase of expression highlighted with white arrowheads and decrease with black arrowheads. Numbers in parentheses indicate the number of embryos analyzed for each condition.

See also [Figures S4](#) and [S5](#).

co-injection of full-length *pkd2* mRNA ([Figures 4F](#) and [S4A–S4C](#)). As reported, calcium spikes during gastrulation were dependent on intracellular calcium ([Wallingford et al., 2001](#)), and we treated embryos again with Tg. To test whether *foxj1* expression was dependent on calcium dynamics as well, specimens were treated with brief pulses (maximum 20 min) at stage 9, when *foxj1* expression is initiated before the start of gastrulation. Treated embryos developed without gastrulation defects but showed a lack of *pitx2c* expression in more than 60% of cases, reminiscent of *pkd2* morphants ([Figures S4D–S4F](#)). When such specimens were analyzed at the onset of gastrulation (st. 10.5), *foxj1* was reduced or absent as well, confirming a requirement of both calcium-dependent signals and Polycystin-2 for *foxj1* induction ([Figures 4G–4I](#)). Surprisingly, in our hands, similar incubations during the initiation of *foxj1* expression (late blastula st. 9 until early gastrula st. 10.5) using the calcium-chelator BAPTA-AM did not alter *foxj1* expression ([Figures S4G–S4I](#)). Accordingly, such treated embryos did not show LR axis alterations at tail bud stages, as shown by wild-type *pitx2c* expression ([Figure S4J](#)). However, embryos incubated in BAPTA-AM from late blastula (st. 9) to late gastrula stages (st. 12.5), i.e., additionally covering the later sensitive time window of *nodal1* initiation in the lateral GRP (cf. [Figures S3J–S3P](#)), again developed laterality defects by misexpression of *pitx2c* ([Figure S4J](#)). These results suggested that Polycystin-2/Tg and BAPTA-AM have different effects on the process of *foxj1* induction. Yet, in sum, these experiments are in line with a function for *pkd2* and specific calcium changes in the specification of the SM as the LRO precursor tissue.

***pkd2* Synergizes with *xnr3* to Induce *foxj1* in the Superficial Mesoderm**

Little is known about early signaling pathways that set up the SM. We and others previously demonstrated that canonical Wnt signaling, which depends on type 3 serotonin receptor signaling (Htr3) in the SM, was required for the induction of both *xnr3* and *foxj1* ([Beyer et al., 2012](#)). In that light, the above-mentioned up-regulation of *xnr3* in *pkd2* morphants ([Figures 4A–4C](#)) argued against the participation of Polycystin-2 as part of the Wnt signaling module upstream of *xnr3* and *foxj1*. To verify this, we analyzed whether *pkd2* was required for Wnt-dependent secondary axis induction. Twinning was induced by ventral injection of *wnt8* mRNA, in the presence or absence of Pkd2-MO. Inhibition of Polycystin-2 did not affect the frequency of secondary axis formation ([Figures S5A–S5C](#)), nor did it affect endogenous organizer gene expression (not shown). Polycystin-2, thus, should not be part of upstream canonical Wnt signaling but control *foxj1* induction in the SM independently.

The opposing effects of *pkd2* knockdown on *foxj1* and *xnr3* made us wonder whether the effect on *foxj1* was mediated through Xnr3. This nodal-related gene is unusual, as it does not interact with TGF- β -type receptors but interacts with Fgf receptor 1 (Fgfr1); MO-mediated *xnr3* knockdown specifically inhibits *brachyury* expression ([Yokota et al., 2003](#)). Besides serving as an SM marker gene, this *Xenopus*-specific factor has not been investigated for a possible function in the context of LR asymmetry. To test whether Xnr3 played a role in laterality determination, we targeted the Xnr3-MO to the dorsal midline (organizer and SM). Knockdown resulted in loss of dorsal *brachyury* expression, as described previously ([Figures S5D–S5F](#); [Yokota et al., 2003](#)). Strikingly, when such specimens were analyzed for *foxj1*, expression in the SM was also lost or strongly reduced as compared with control embryos ([Figures 4J, 4K, and 4O](#)). This phenotype was specific to loss of Xnr3 function, as reintroduction of full-length *xnr3*-mRNA, which is insensitive to the Xnr3-MO, was able to rescue the observed reduction of *foxj1* very efficiently ([Figures 4L and 4O](#)). Morphants that were raised further revealed the previously reported convergent extension defects ([Yokota et al., 2003](#)) and altered *pitx2c* expression (data not shown).

Conversely, when *xnr3* was overexpressed in the dorsal SM, an increase of *foxj1* expression was observed, specifically in the more lateral part of the expression domain, the future lateral GRP, demonstrating that Xnr3 was able to enhance *foxj1* expression ([Figures 4M and 4O](#)). Interestingly, injecting *xnr3* mRNA into the ventral side was sufficient to induce *foxj1* expression ectopically, demonstrating its role in SM fate

specification (Figures 4N and 4O). This could indicate a potential role of the well-characterized ventral Bmp signaling pathway in preventing the activation of *foxf1* in the ventral superficial layer, as it has been shown that Xnr3 itself has a dorsalizing effect by inhibiting Bmp signaling (Hansen et al., 1997; Haramoto et al., 2004). Thus, to finally test whether *xnr3* and *pkd2* synergized in SM *foxf1* induction, we performed epistasis experiments. MO doses for both genes were reduced such that individually they did not result in a strong reduction of *foxf1* expression. Combined injection of Pkd2-MO and Xnr3-MO, however, resulted in a strong reduction or loss of *foxf1*, establishing a genetic interaction of these genes in SM *foxf1* induction and, thus, in setting up a functional LRO (Figures 4O–4S). Interestingly, although exogenously introduced *pkd2* mRNA caused an increase of *foxf1* expression (Figure S4C), it was not sufficient to rescue *foxf1* expression in *xnr3* morphant specimens (data not shown).

In summary, our data demonstrate that in general terms, *pkd2* is a conserved determinant of LR symmetry breakage in *Xenopus*. Surprisingly, however, *pkd2* is strictly required upstream of leftward flow to set up the LRO during gastrulation, together with *xnr3* (Figure 4T). Polycystin2 in the future SM cells could provide a crucial signal for specification. However, the protein of such cell-autonomous function should be of maternal origin, particularly because zygotic mRNA was not detected in the LR-relevant tissues, SM and GRP. Alternatively, Pkd2 could act non-cell autonomously in the deep tissue to induce *foxf1* in the superficial layer, i.e., indirectly. It remains to be seen which type of activating signal could mediate this induction. Based on our timed Tg treatments at the blastula or late gastrula stages (Figures 4G–4I and S3J–S3L), and the corresponding central or lateral Pkd2-MO injections (Figures 3M and 4E, respectively), which resulted in either loss of *foxf1* or loss of *nodal1*, respectively, the following conclusion can be drawn. These differentiable results from two different time points of LR symmetry breakage imply that both Pkd2 function and intracellular calcium changes are necessary at two separate steps of LRO induction and sub-functionalization in *Xenopus* (Figure 4T). It remains to be seen which other signaling pathways could be required for each of these steps.

In any way, we propose that in evolutionary terms, this may represent an ancestral Polycystin-2 function in amphibian embryos, which undergo a basal mode of vertebrate gastrulation and thus LRO development (Blum et al., 2009; Cooper and Virta, 2007). Interestingly, zebrafish morphant but not mutant embryos display early mesendodermal defects after maternal *pkd2* knockdown, reminiscent of SM loss in *Xenopus* (Schottenfeld et al., 2007). It is tempting to speculate that Fgf signaling represents the common denominator in this context, as Xnr3 binds and signals via the Fgfr1 (Yokota et al., 2003). In zebrafish, Fgfr1 signaling affects *foxf1* expression, LRO ciliogenesis, and flow (Neugebauer et al., 2009). In mouse embryos, early loss of Fgfr1-mediated signaling results in gastrulation defects, but *pkd2*-knockout mice do not display impaired LRO formation or flow (Yamaguchi et al., 1994; Yoshida et al., 2012). Treatment with an Fgfr1 inhibitor, however, blocked *nodal* expression in lateral LRO cells (Oki et al., 2010) in much the same way as observed upon loss of *pkd2* in *Xenopus*. Thus, LRO induction, although still dependent on Fgfr1, may have become independent of (maternal) *pkd2* in modern bony fish and mammals. The later role of Polycystin-2 in flow sensing at the lateral LRO cells may very well be conserved in amphibians as well. The loss of LRO and flow in *pkd2* morphants precluded the analysis in the context of the present study. The novel role ascribed to Polycystin-2 in Xnr3-/FGF-dependent LRO morphogenesis adds to the long list of functions of this factor that is conserved in animals from nematodes to humans.

METHODS

All methods can be found in the accompanying [Transparent Methods supplemental file](#).

SUPPLEMENTAL INFORMATION

Supplemental Information includes Transparent Methods, five figures, and one video and can be found with this article online at <https://doi.org/10.1016/j.isci.2018.03.011>.

ACKNOWLEDGMENTS

M.B. was funded by the Deutsche Forschungsgemeinschaft (BL285/9-2). J.K. and M.G. were recipients of a Ph.D. fellowship from the Landesgraduiertenförderung Baden-Württemberg. We thank Susanne Bogusch, Anna Schäfer, Sabrina Kurz, and Verena Andre for technical assistance, Kathrin Ott for help with double axis assay and IF experiments, and C. Kintner, A. Brivanlou, and J. Heasman for plasmids.

AUTHOR CONTRIBUTIONS

P.V., M.B., and A.S. conceived, designed, and supervised the experiments; P.V., J.K., I.S., M.T., M.G., T.T., and T.B. performed and analyzed the experiments; P.V. and A.S. interpreted results; and P.V. wrote the original and the revised manuscript with the help of M.B. and final input of all authors.

DECLARATION OF INTERESTS

The authors declare no competing interest.

Received: November 21, 2017

Revised: February 15, 2018

Accepted: February 28, 2018

Published: April 27, 2018

REFERENCES

- Beyer, T., Danilchik, M., Thumberger, T., Vick, P., Tisler, M., Schneider, I., Bogusch, S., Andre, P., Ulmer, B., Walentek, P., et al. (2012). Serotonin signaling is required for Wnt-dependent GRP specification and leftward flow in *Xenopus*. *Curr. Biol.* 22, 33–39.
- Bigrove, B.W., Snarr, B.S., Emrazian, A., and Yost, H.J. (2005). Polaris and Polycystin-2 in dorsal forerunner cells and Kupffer's vesicle are required for specification of the zebrafish left-right axis. *Dev. Biol.* 287, 274–288.
- Blum, M., Feistel, K., Thumberger, T., and Schweickert, A. (2014a). The evolution and conservation of left-right patterning mechanisms. *Development* 141, 1603–1613.
- Blum, M., Schweickert, A., Vick, P., Wright, C.V.E., and Danilchik, M.V. (2014b). Symmetry breakage in the vertebrate embryo: when does it happen and how does it work? *Dev. Biol.* 393, 109–123.
- Blum, M., Weber, T., Beyer, T., and Vick, P. (2009). Evolution of leftward flow. *Semin. Cell. Dev. Biol.* 20, 464–471.
- Busch, T., Köttgen, M., and Hofherr, A. (2017). TRPP2 ion channels: critical regulators of organ morphogenesis in health and disease. *Cell Calcium* 66, 25–32.
- Cooper, M.S., and Virta, V.C. (2007). Evolution of gastrulation in the ray-finned (actinopterygian) fishes. *J. Exp. Zool.* 308B, 591–608.
- Essner, J.J., Amack, J.D., Nyholm, M.K., Harris, E.B., and Yost, H.J. (2005). Kupffer's vesicle is a ciliated organ of asymmetry in the zebrafish embryo that initiates left-right development of the brain, heart and gut. *Development* 132, 1247–1260.
- Futel, M., Leclerc, C., Le Bouffant, R., Buisson, I., Néant, I., Umbhauer, M., Moreau, M., and Riou, J.-F. (2015). TRPP2-dependent Ca²⁺ signaling in dorso-lateral mesoderm is required for kidney field establishment in *Xenopus*. *J. Cell Sci.* 128, 888–899.
- Glinka, A., Delius, H., Blumenstock, C., and Niehrs, C. (1996). Combinatorial signalling by *Xwnt-11* and *Xnr3* in the organizer epithelium. *Mech. Dev.* 60, 221–231.
- Grimes, D.T., and Burdine, R.D. (2017). Left-right patterning: breaking symmetry to asymmetric morphogenesis. *Trends Genet.* 33, 616–628.
- Hansen, C.S., Marion, C.D., Steele, K., George, S., and Smith, W.C. (1997). Direct neural induction and selective inhibition of mesoderm and epidermis inducers by *Xnr3*. *Development* 124, 483–492.
- Haramoto, Y., Tanegashima, K., Onuma, Y., Takahashi, S., Sekizaki, H., and Asashima, M. (2004). *Xenopus tropicalis* nodal-related gene 3 regulates BMP signaling: an essential role for the pro-region. *Dev. Biol.* 265, 155–168.
- McGrath, J., Somlo, S., Makova, S., Tian, X., and Brueckner, M. (2003). Two populations of node monocilia initiate left-right asymmetry in the mouse. *Cell* 114, 61–73.
- Namigai, E.K.O., Kenny, N.J., and Shimeld, S.M. (2014). Right across the tree of life: the evolution of left-right asymmetry in the Bilateria. *Genesis* 52, 458–470.
- Neugebauer, J.M., Amack, J.D., Peterson, A.G., Bigrove, B.W., and Yost, H.J. (2009). FGF signalling during embryo development regulates cilia length in diverse epithelia. *Nature* 458, 651–654.
- Nonaka, S., Tanaka, Y., Okada, Y., Takeda, S., Harada, A., Kanai, Y., Kido, M., and Hirokawa, N. (1998). Randomization of left-right asymmetry due to loss of nodal cilia generating leftward flow of extraembryonic fluid in mice lacking KIF3B motor protein. *Cell* 95, 829–837.
- Oki, S., Kitajima, K., and Meno, C. (2010). Dissecting the role of Fgf signaling during gastrulation and left-right axis formation in mouse embryos using chemical inhibitors. *Dev. Dyn.* 239, 1768–1778.
- Pennekamp, P., Karcher, C., Fischer, A., Schweickert, A., Skryabin, B., Horst, J., Blum, M., and Dworniczak, B. (2002). The ion channel polycystin-2 is required for left-right axis determination in mice. *Curr. Biol.* 12, 938–943.
- Sarmah, B., Latimer, A.J., Appel, B., and Wente, S.R. (2005). Inositol polyphosphates regulate zebrafish left-right asymmetry. *Dev. Cell.* 9, 133–145.
- Sáenz-Ponce, N., Santillana-Ortiz, J.-D., and del Pino, E.M. (2011). The gastrocoel roof plate in embryos of different frogs. *Differentiation* 83, S62–S66.
- Schottenfeld, J., Sullivan-Brown, J., and Burdine, R.D. (2007). Zebrafish curly up encodes a Pkd2 ortholog that restricts left-side-specific expression of southpaw. *Development* 134, 1605–1615.
- Schweickert, A., Vick, P., Getwan, M., Weber, T., Schneider, I., Eberhardt, M., Beyer, T., Pachur, A., and Blum, M. (2010). The nodal inhibitor coco is a critical target of leftward flow in *Xenopus*. *Curr. Biol.* 20, 738–743.
- Schweickert, A., Weber, T., Beyer, T., Vick, P., Bogusch, S., Feistel, K., and Blum, M. (2007). Cilia-driven leftward flow determines laterality in *Xenopus*. *Curr. Biol.* 17, 60–66.
- Shinohara, K., Kawasumi, A., Takamatsu, A., Yoshida, S., Botilde, Y., Motoyama, N., Reith, W., Durand, B., Shiratori, H., and Hamada, H. (2012). Two rotating cilia in the node cavity are sufficient to break left-right symmetry in the mouse embryo. *Nat. Commun.* 3, 622.
- Shiratori, H., and Hamada, H. (2014). TGF β signaling in establishing left-right asymmetry. *Semin. Cell. Dev. Biol.* 32, 80–84.
- Smith, W.C., McKendry, R., Ribisi, S., and Harland, R.M. (1995). A nodal-related gene defines a physical and functional domain within the Spemann organizer. *Cell* 82, 37–46.
- Stubbs, J.L., Oishi, I., Izpisua-Belmonte, J.C., and Kintner, C. (2008). The forkhead protein *Foxj1* specifies node-like cilia in *Xenopus* and zebrafish embryos. *Nat. Genet.* 40, 1454–1460.
- Sullivan-Brown, J., Schottenfeld, J., Okabe, N., Hostetter, C.L., Serluca, F.C., Thiberge, S.Y., and Burdine, R.D. (2008). Zebrafish mutations affecting cilia motility share similar cystic phenotypes and suggest a mechanism of cyst formation that differs from *pkd2* morphants. *Dev. Biol.* 314, 261–275.
- Tabin, C.J., and Vogan, K.J. (2003). A two-cilia model for vertebrate left-right axis specification. *Genes Dev.* 17, 1–6.
- Takao, D., Nemoto, T., Abe, T., Kiyonari, H., Kajjura-Kobayashi, H., Shiratori, H., and Nonaka, S.

(2013). Asymmetric distribution of dynamic calcium signals in the node of mouse embryo during left-right axis formation. *Dev. Biol.* 376, 23–30.

Thastrup, O., Cullen, P.J., Drøbak, B.K., Hanley, M.R., and Dawson, A.P. (1990). Thapsigargin, a tumor promoter, discharges intracellular Ca²⁺ stores by specific inhibition of the endoplasmic reticulum Ca²⁺-ATPase. *Proc. Natl. Acad. Sci. USA* 87, 2466–2470.

Tisler, M., Wetzel, F., Mantino, S., Kremnyov, S., Thumberger, T., Schweickert, A., Blum, M., and Vick, P. (2016). Cilia are required for asymmetric nodal induction in the sea urchin embryo. *BMC Dev. Biol.* 16, 28.

Tran, U., Zakin, L., Schweickert, A., Agrawal, R., Doger, R., Blum, M., De Robertis, E.M., and Wessely, O. (2010). The RNA-binding protein bicaudal C regulates polycystin 2 in the kidney by antagonizing miR-17 activity. *Development* 137, 1107–1116.

Vick, P., Schweickert, A., Weber, T., Eberhardt, M., Mencl, S., Shcherbakov, D., Beyer, T., and Blum, M. (2009). Flow on the right side of the gastrocoel roof plate is dispensable for symmetry breakage in the frog *Xenopus laevis*. *Dev. Biol.* 331, 281–291.

Walentek, P., Schneider, I., Schweickert, A., and Blum, M. (2013). Wnt11b is involved in cilia-mediated symmetry breakage during *Xenopus* left-right development. *PLoS One* 8, e73646–e73649.

Wallingford, J.B., Ewald, A.J., Harland, R.M., and Fraser, S.E. (2001). Calcium signaling during convergent extension in *Xenopus*. *Curr. Biol.* 11, 652–661.

Yamaguchi, T.P., Harpal, K., Henkemeyer, M., and Rossant, J. (1994). *fgfr-1* is required for embryonic growth and mesodermal patterning during mouse gastrulation. *Genes Dev.* 8, 3032–3044.

Yokota, C., Kofron, M., Zuck, M., Houston, D.W., Isaacs, H., Asashima, M., Wylie, C.C., and Heasman, J. (2003). A novel role for a nodal-related protein; Xnr3 regulates convergent extension movements via the FGF receptor. *Development* 130, 2199–2212.

Yoshida, S., and Hamada, H. (2014). Roles of cilia, fluid flow, and Ca²⁺ signaling in breaking of left-right symmetry. *Trends Genet.* 30, 10–17.

Yoshida, S., Shiratori, H., Kuo, I.Y., Kawasumi, A., Shinohara, K., Nonaka, S., Asai, Y., Sasaki, G., Belo, J.A., Sasaki, H., et al. (2012). Cilia at the node of mouse embryos sense fluid flow for left-right determination via Pkd2. *Science* 338, 226–231.

Yuan, S., Zhao, L., Brueckner, M., and Sun, Z. (2015). Intraciliary calcium oscillations initiate vertebrate left-right asymmetry. *Curr. Biol.* 25, 556–567.

ISCI, Volume 2

Supplemental Information

An Early Function of Polycystin-2 for Left-Right Organizer Induction in *Xenopus*

Philipp Vick, Jennifer Kreis, Isabelle Schneider, Melanie Tingler, Maike Getwan, Thomas Thumberger, Tina Beyer, Axel Schweickert, and Martin Blum

Supplemental Figures and legends

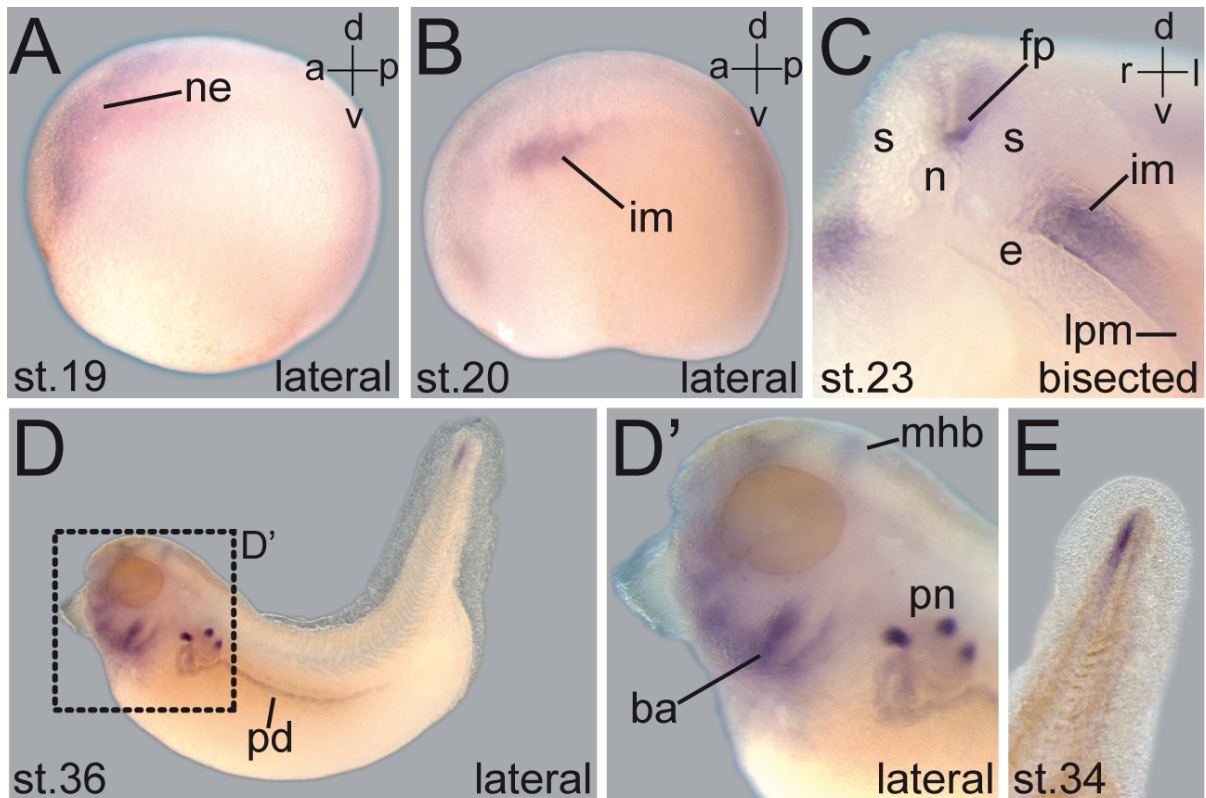


Figure S1: Related to Figure 1. Late expression pattern of *pkd2*.

Expression in the neuroectoderm (A-C), intermediate mesoderm (B, C), pronephric system (D), branchial arches (D') and tailbud (E) in early to late tailbud stages.

a, anterior; ba, branchial arches; d, dorsal; e, endoderm; fp, floorplate; im, intermediate mesoderm; l, left; lpm, lateral plate mesoderm; mhb, mid hindbrain boundary; n, notochord; ne, neuroectoderm; pd, pronephric duct; pn, pronephros; r, right; s, somites; v, ventral

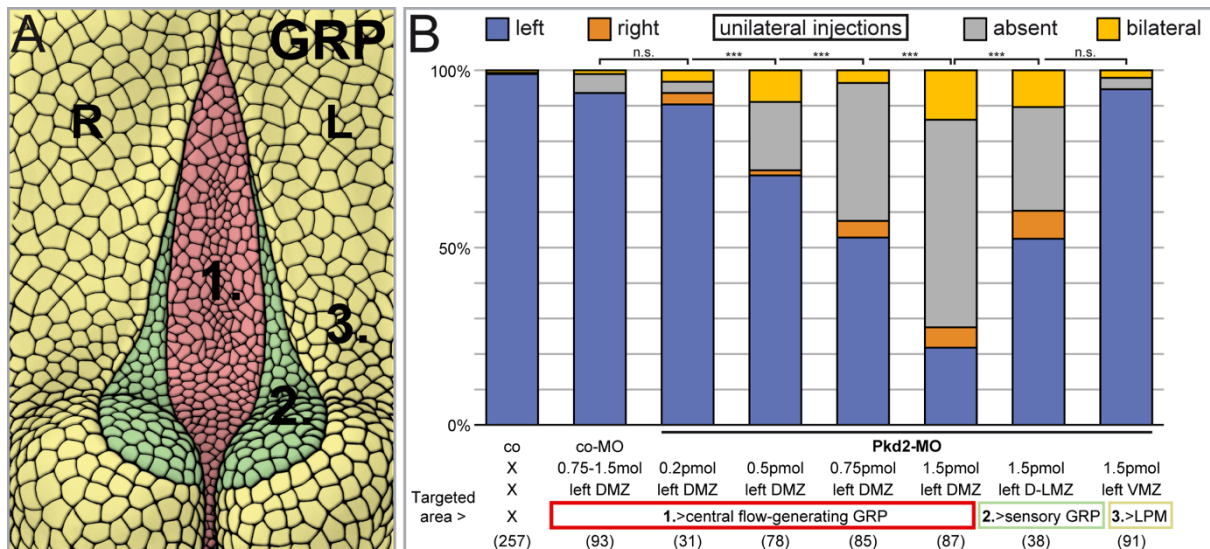


Figure S2: Related to Figure 2. Lineage-specific knockdown of *pkd2* reveals a left-sided dorsal requirement of Polycystin-2 in the LRO

(A) Schematic depiction of the differentially targeted areas of the gastrocoel roof in a dorsal explant of a stage 17 neurula embryo with the central, flow-generating population of the LRO (1. red), the lateral, sensory population of the LRO (2. green), and the surrounding endodermal cells (3. yellow) that cover the lateral plate mesoderm, which will express *nodal* and *pitx2c* on the left side after flow-dependent symmetry breakage to govern asymmetric organogenesis.

(B) Unilateral left-sided *pkd2* knockdown experiment showing dose-dependent loss of *pitx2c* when injected into the left dorsal marginal zone (DMZ) to target the central, flow-generating GRP. Injection into the dorso-lateral marginal zone (D-LMZ) to target the sensory part of the GRP (i.e. the lateral LRO cells) caused fewer, yet significant LR defects. Injecting the ventral marginal zone (VMZ) to target the left lateral plate mesoderm did not result in miss-expression of *pitx2c*.

* $p < 0.05$, ** $p < 0.01$, *** $p < 0.001$ for all panels.

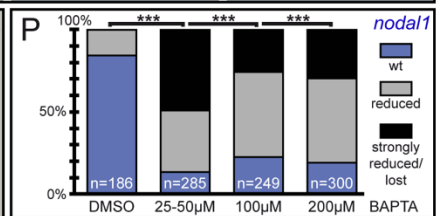
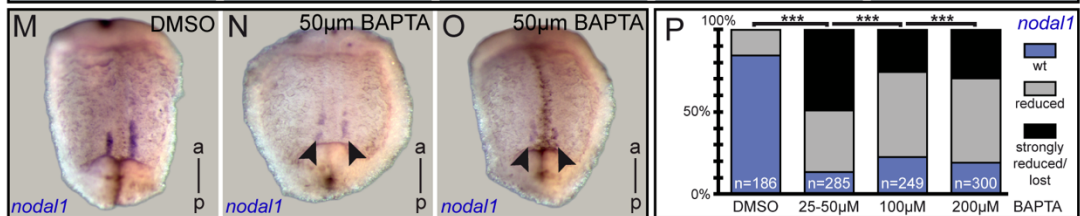
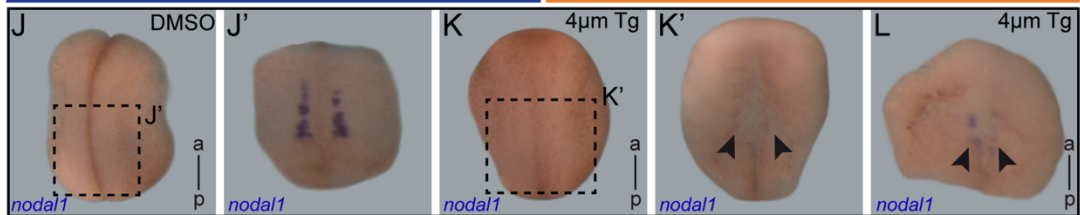
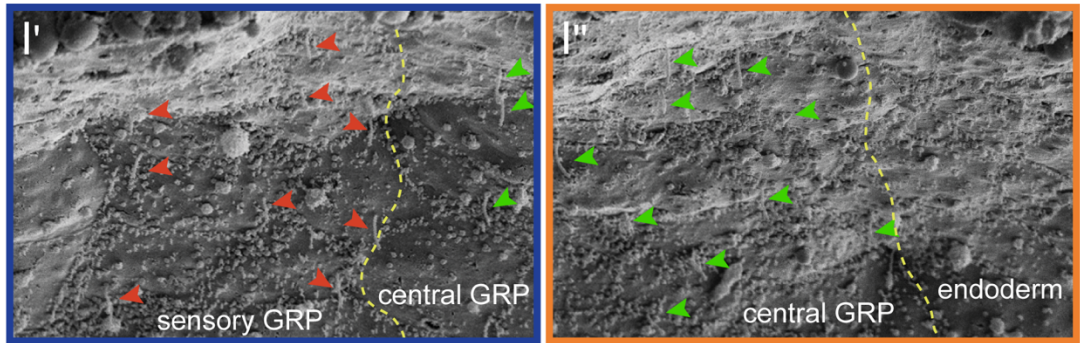
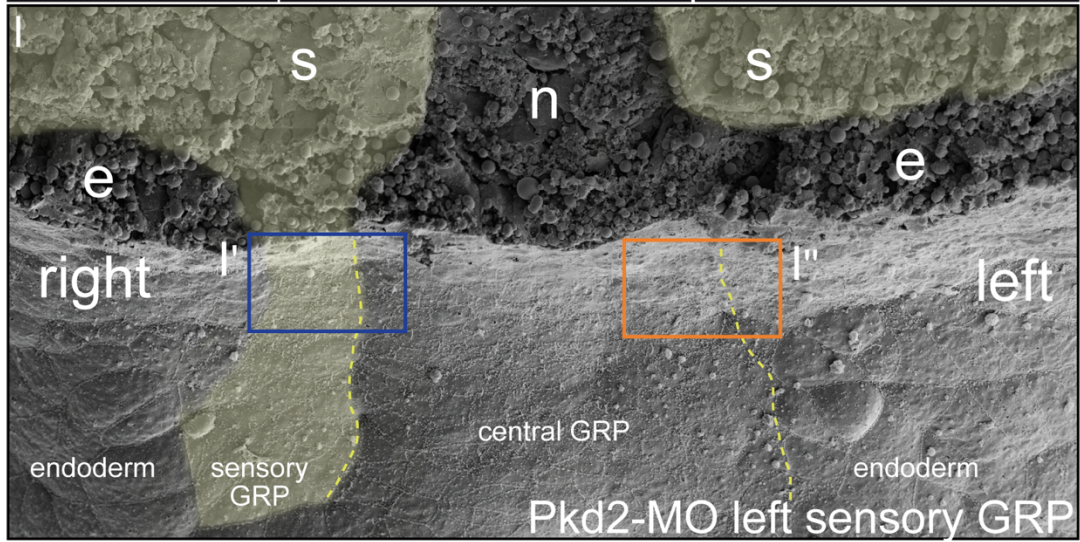
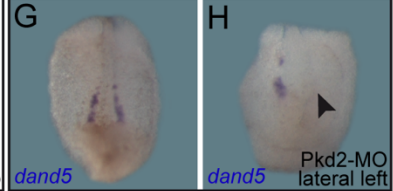
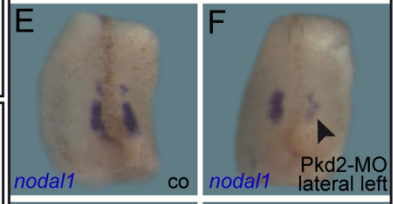
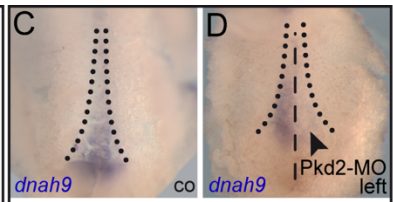
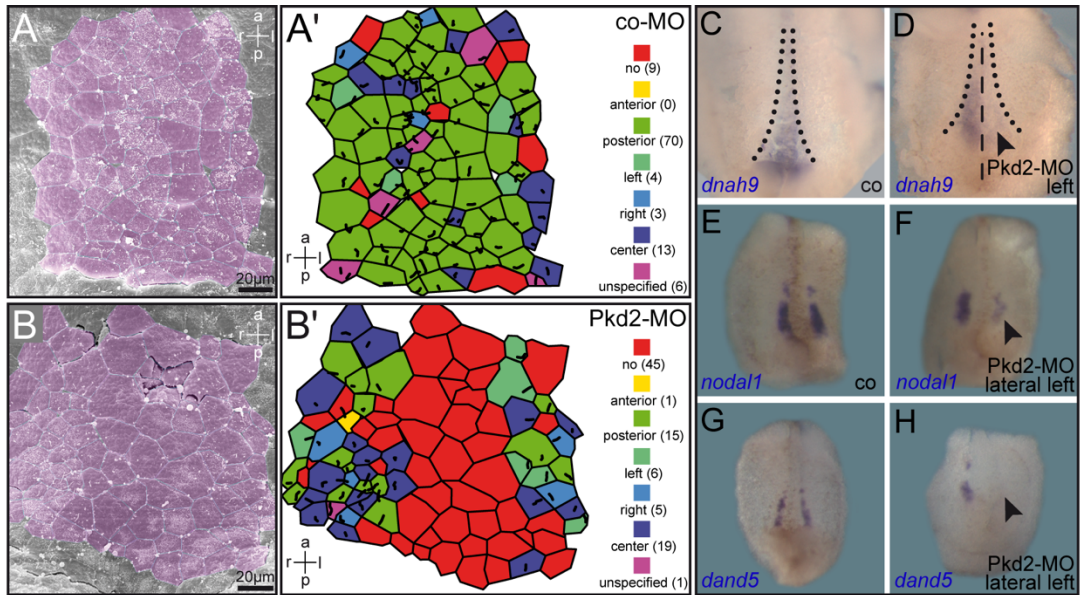


Figure S3: Related to Figure 3. GRP defects in *pkd2* morphants

(A, B) SEM analysis of co-MO (A) and Pkd2-MO (B) injected specimens reveal loss of ciliation and altered GRP cell morphology in morphants. Examples are representative for 6 specimens analyzed each. Scale bars represent 20 micrometers.

(C-H) Unilateral absence of *dnah9* (D), *nodal1* (F) and *dand5* (H) in left-injected embryos in comparison to internal control sides at stage 17. Control embryos (C, E, G) show wildtype expression levels.

(I) SEM analysis of ciliation and cell morphology in dorsal explant of stage 17 specimen unilaterally injected with Pkd2-MO targeted exclusively to the lateral, sensory part of the GRP. Shown is a ventral view of the GRP broken transversally and revealing the deep tissue arrangements in the top half of the picture. Right (I') and left (I'') magnifications show both the sensory areas of the GRP. Note that the lateral GRP cells were absent on the MO-injected side, such that central GRP cells, which are characterized by posteriorly polarized cilia, directly bordered non-ciliated endodermal cells. Sensory GRP cilia highlighted with red arrowheads, central GRP cilia with green arrowheads.

(J-L) Expression of *nodal1* in lateral GRP cells of flow stage (st. 17) specimens following Tp (K, L) or 1% DMSO (J) treatment during mid to late gastrula stage (st. 11.5). *nodal1* was lost (K') or strongly reduced (L) after Tp treatment, without causing gastrulation defects.

(M-P) Expression of *nodal1* in lateral GRP cells of flow stage (st. 16-19) specimens following 25-200 μ M BAPTA-AM (N-P) or 0.05-1% DMSO (M, P) treatment during mid and late gastrula stages (st. 11.5-13/14). *nodal1* was lost (O) or reduced (N) after BAPTA-AM treatment.

* $p < 0.05$, ** $p < 0.01$, *** $p < 0.001$

Black arrowheads indicate reduction or lack of expression.

a, anterior; e, endoderm; l, left; n, notochord; p, posterior; r, right; s, somites

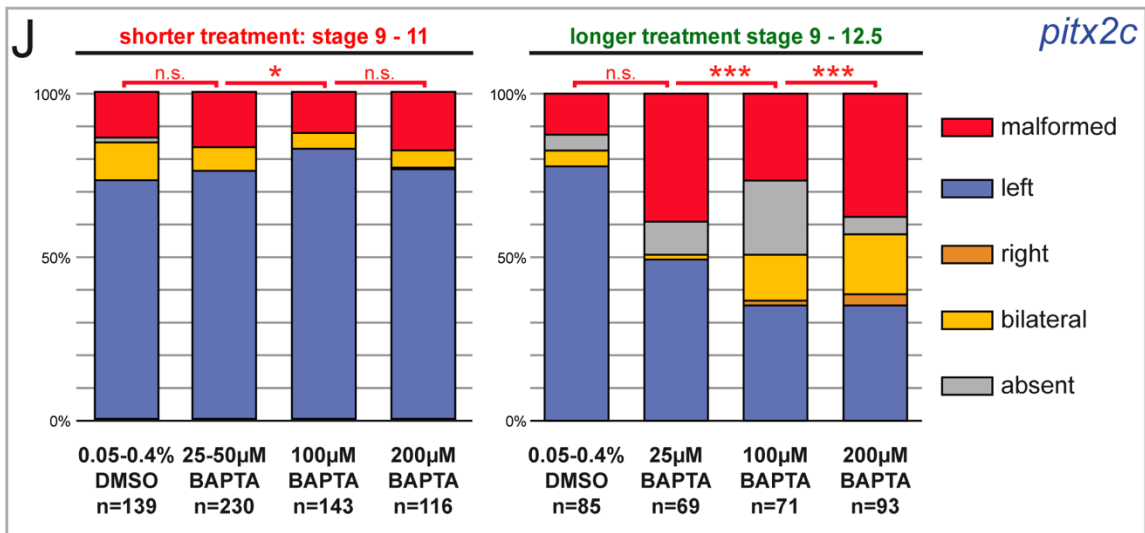
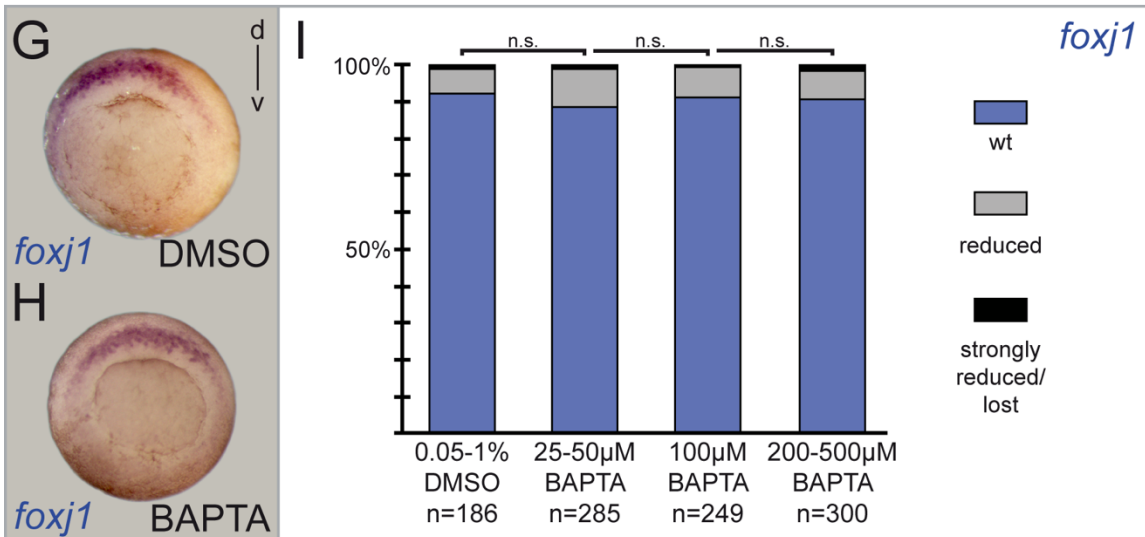
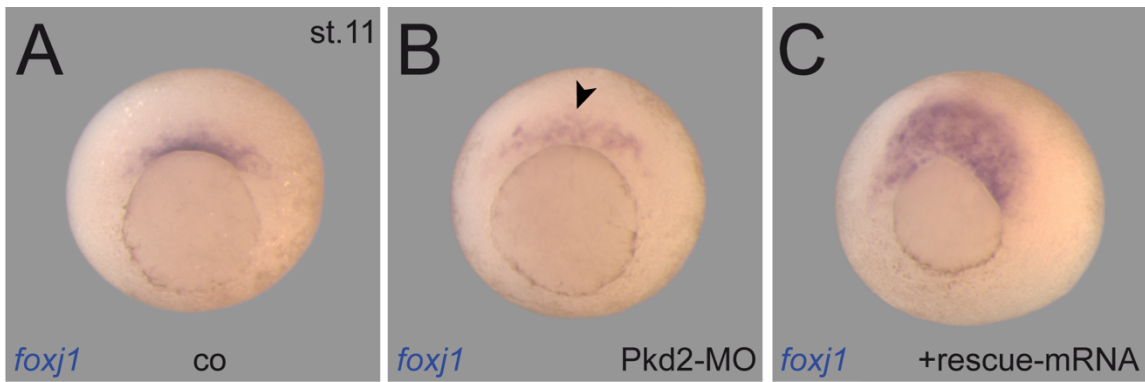


Figure S4: Related to Figure 4. Calcium manipulating agents Thapsigargin or BAPTA-AM impacted differently on LR development

(A-C) *foxj1* expression (A) was reduced in *pkd2* morphants (B) and rescued upon co-injection of Pkd2-MO and a full-length *pkd2* rescue mRNA not targeted by the MO (C).

(D-F) A 20-minute thapsigargin treatment before gastrulation resulted in loss of *pitx2c* expression in >50% of embryos without concomitant gastrulation defects, reminiscent of Pkd2-MO injected specimens (cf. Figure 2D).

(G-J) Treatment of embryos between blastula (st. 9) and early gastrula stages (st. 10.5) with different concentrations of the calcium chelator BAPTA-AM did not reduce *foxj1* expression (H, I), in comparison to 0.05-1.00% DMSO treatment (G, I). (J) Embryos analyzed for *pitx2c* expression at tailbud stages after short (left side, until stage 11) or long (right side, until stage 12.5) treatment with BAPTA-AM. Longer (st. 9-12.5), but not short treatment (st. 9-11) resulted in significant LR defects. Please note the high proportion of embryos with general axis malformations when treated until late gastrulation (right side) as compared to shorter treatment (left side). Significances in (J) were calculated for LR expression patterns of *pitx2c* only, not including malformed embryos, which are also shown in the graph.

* $p < 0.05$, ** $p < 0.01$, *** $p < 0.001$ for all panels.

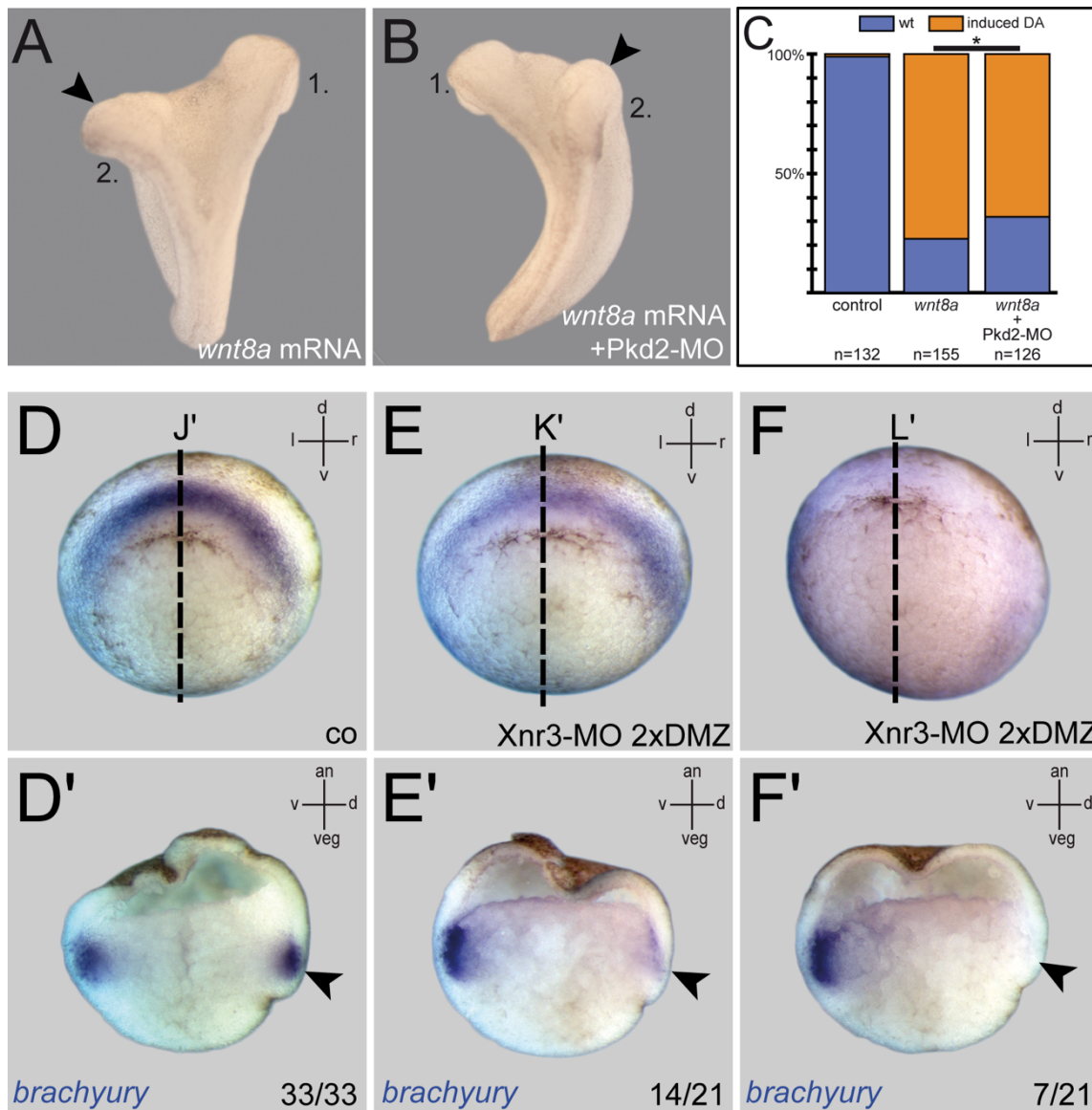


Figure S5: Related to Figure 4. Polycystin-2 function in LR axis formation is independent of canonical Wnt signaling

(A-C) Wnt-dependent double axis formation. Injection of *wnt8a* mRNA resulted in >75% of conjoined twinning (A, C). Co-injection of Pkd2-MO resulted in a very moderate drop of twinning rates to approx. 70% (B, C). Quantification of results (C). Arrowhead indicates induced secondary axis.

(D-F) Wildtype expression of *brachyury* during gastrulation in control specimens (D) was reduced (E) or lost (F) after injection of Xnr3-MO into the dorsal marginal zone (DMZ), demonstrating that Xnr3 was required for dorsal *bra* expression. Bisected embryos in D', E' and F' highlight these effects.

TRANSPARENT METHODS

CONTACT FOR REAGENT AND RESOURCE SHARING

Further information and requests for resources and reagents should be directed to and will be fulfilled by the Lead Contact, Philipp Vick (philipp.vick@uni-hohenheim.de).

EXPERIMENTAL MODEL AND SUBJECT DETAIL

For *in vivo* studies, *Xenopus laevis* was used as model organism. Frogs were obtained from Nasco (901 Janesville Avenue P.O. Box 901 Fort Atkinson). Handling, care and experimental manipulations of animals was approved by the Regional Government Stuttgart, Germany (Vorhaben A379/12 ZO „Molekulare Embryologie“), according to German regulations and laws (§6, article 1, sentence 2, nr. 4 of the animal protection act). Animals were kept at the appropriate condition (pH=7.7, 20°C) at a 12 h light cycle in the animal facility of the Institute of Zoology of the University of Hohenheim. Female frogs (4-20 years old) were stimulated with 25-75 units of human chorionic gonadotropin (hCG; Sigma), depending on weight and age, that was injected subcutaneously one week prior to oviposition. On the day prior to ovulation, female frogs were injected with 300-700 units of hCG (10-12 h before). Eggs were collected into a petri dish by carefully squeezing of the females and *in vitro* fertilized. Sperm of male frogs was gained by dissecting of the testes that was stored at 4°C in 1x MBSH (Modified Barth`s saline with HEPES) solution.

METHOD DETAILS

Plasmid construction

For *xnr3* mRNA-rescue experiments, the *xnr3* coding sequence was isolated from the original plasmid using Pfu DNA polymerase and sub-cloned into the CS2+ plasmid with EcoRI and XhoI restriction sites with the following oligonucleotides for PCR:

Xnr3.1 forward primer: 5' CCGGAATTCATGGCATTCTGAACCTG 3'
Xnr3.1 reverse primer: 5' CCGCTCGAGTTACATGTCCTTGAATCC 3'

For *in vitro* synthesis of mRNA using the Ambion sp6 message kit, the plasmid was linearized with NotI.

Microinjections

Embryos were injected at the 4- to 8-cell stage, using a Harvard Apparatus. Drop size was calibrated to 4-6 nl / injection, amounts of injected MOs are indicated in the main text. Lineage tracers used for injection control were fluorescein (70,000 MW) or rhodamine B dextran (10,000 MW; both ThermoFisher). More detailed lineage-specific injections to target GRP and ventro-lateral tissues have been described previously (Blum et al., 2009a).

Treatments with calcium inhibitors

To manipulate intracellular calcium levels and wave patterns, embryos were incubated at two different time points, either with the ER SERCA-pump inhibitor Thapsigargin, or

with BAPTA-AM (cell-permeable form of the calcium-chelator BAPTA), both diluted in 0.1x MBSH.

For *foxj1* induction, embryos were incubated at stage 9 (before start of gastrulation) for 10, 15 or 20 min in 2 μ M Tg, then solution was replaced by 0.1x MBSH and embryos fixed at stage 10.5. Most robust effects were obtained with 15 or 20 min treatments, longer treatments with this concentration started to impact on gastrulation. Alternatively, ca. 120 min treatment with 0.75 μ M caused similar results (not shown). A similar procedure was applied for BAPTA-AM but solution was not replaced until fixation at stage 10.5 (begin of gastrulation). Tested concentration range was as indicated in Figure S4.

For analysis of *nodal1* induction, embryos were incubated in 4 μ M Tg, or in BAPTA-AM as indicated in Figure S3, both from stage 11.5 on to avoid gastrulation defects, and embryos were fixed at stage 15-18 (during flow-stages) for analysis by ISH.

For complementary *pitx2c* analyses, some embryos were reared until tailbud stages and processed for ISH after washout of the drug.

Immunofluorescence staining

For immunofluorescence staining, embryos were fixed in 4% PFA (Polyoxymethylene) for 1h at RT on a rocking platform, followed by 2 washes in 1x PBS⁻ for 15 min each. For staining of GRP explants, embryos were manually dissected transversally using a razor blade. Posterior halves (GRP explants) were collected and transferred to a 24 well plate and washed twice for 15 min in PBST. GRP-explants and whole embryos were blocked for 2h at RT in CAS-Block diluted 1:10 in PBST (0.1% Triton X-100). The blocking reagent was replaced by antibody solution (anti-acetylated tubulin antibody, 1:700 in CAS-Block) and incubated ON at 4°C. Antibody solution was removed and explants washed twice for 15 min in PBS, then the secondary antibody (1:1000 in CAS-Block) was added. Alexa Fluor 488 Phalloidin (1:200) was incubated over-night. Before photo documentation with a Zeiss LSM 700 Axioplan2 Imaging microscope, embryos or explants were shortly washed in PBS⁻ and transferred onto a microscope slide.

SEM and GRP Analysis

co-MO or Pkd2-MO injected specimens were fixed with 4% paraformaldehyde/ 2.5% glutaraldehyde and processed for SEM analysis. SEM photographs were analyzed for ciliation, polarization and cell surface area by individual full GRP analysis using ImageJ and evaluated as described (Beyer et al., 2012; Sbalzarini and Koumoutsakos, 2005).

Whole-mount in situ hybridization (ISH)

Embryos were fixed in MEMFA for 2h and processed following standard protocols (Sive et al., 2000). RNA *in situ* probes were transcribed using SP6 or T7 polymerases. In situ hybridization was modified from (Belo et al., 1997).

Flow-analysis

For analysis of leftward flow, dorsal posterior GRP-explants were dissected from stage 16/17 embryos injected with Pkd2-MO/co-MO and the lineage tracer rhodamine-B dextran (0.5 mg/ml) into one or two dorsal blastomeres. GRP-explants were placed in a petri-dish containing fluorescent microbeads (diameter 0.5 μ m; diluted 1:2500 in

1xMBSH) and incubated for a few seconds. Explants were transferred to a microscope slide which was prepared with vacuum grease to create a small chamber that contained fluorescent microbeads solution; a cover slip carefully pressed on to seal the chamber. Time lapse movies of leftward flow were recorded using a AxioCam HSm video camera (Zeiss) at 2 frames per second using an Axioplan2 imaging microscope (Zeiss). For flow analysis, ImageJ and statistical-R, were used. Using the Particle-Tracker plug-in from ImageJ, leftward flow was analyzed and particle movement was measured, and data processed as described previously to create corresponding GTTs (Gradient Time Trails) as shown in Figure 3 (Vick et al., 2009).

Axis induction Assay

Double axis induction was performed by single injection of 40-80pg *wnt8a* mRNA with or without 1pmol Pkd2-MO into one ventral mesodermal blastomere at the 4-8 cell stage. Embryos were cultured until late tailbud stage and scored for double axis induction.

QUANTIFICATION AND STATISTICAL ANALYSIS

Statistical analysis

Statistical calculations of marker gene expression patterns and cilia distribution were performed using Pearson's chi-square test (Bonferroni corrected). For statistical calculation of ciliation, cilia length, cell size, flow velocity and directionality Wilcoxon-Match-Pair test was used (statistical R).

*=p<0.05, **=p<0.01, ***=p<0.001 were used for all statistical analyses.

KEY RESOURCES TABLE

REAGENT or RESOURCE	SOURCE	IDENTIFIER
Antibodies		
Mouse monoclonal anti acetylated α -tubulin	Sigma	AB_477585
Anti-mouse IgG (whole molecule) F(ab') ₂ fragment-Cy3	Sigma	AB_258785
Alexa Fluor 488 Phalloidin	Invitrogen	AB_2315147
Chemicals, Peptides, and Recombinant Proteins		
Pfu DNA Polymerase	Promega	M7745
FluoSpheres™ Carboxylate-Modified Microspheres, 0.5 μ m, yellow-green fluorescent (505/515)	Invitrogen	F8813
Thapsigargin (3 <i>S</i> ,3 <i>aR</i> ,4 <i>S</i> ,6 <i>S</i> ,6 <i>aR</i> ,7 <i>S</i> ,8 <i>S</i> ,9 <i>bS</i>)-6-(Acetyloxy)-4-(butyryloxy)-3,3 <i>a</i> -dihydroxy-3,6,9-trimethyl-8-[[<i>(2Z)</i> -2-methylbut-2-enoyl]oxy]-2-oxo-2,3,3 <i>a</i> ,4,5,6,6 <i>a</i> ,7,8,9 <i>b</i> -decahydroazuleno[4,5- <i>b</i>]furan-7-yl octanoate	Tocris	1138
BAPTA-AM 1,2-Bis(2-aminophenoxy)ethane- <i>N,N,N,N</i> -tetraacetic acid tetrakis(acetoxymethyl ester)	abcam	Ab120503
Human chorionic gonadotropin (hCG)	Sigma	C0809-1VL
Critical Commercial Assays		
mMessage mMachine™ SP6 Transcription Kit	Thermo Fisher Scientific	AM1340
Experimental Models: Organisms/Strains		
<i>Xenopus laevis</i> (female, male)	Nasco	https://www.enasco.com/xenopus/
Oligonucleotides		
Xnr3.1 forward primer [5' CCGGAATTCATGGCATTCTGAACCTG 3']	Sigma	
Xnr3.1 reverse primer [5' CCGCTCGAGTTACATGTCCTTGAATCC 3']	Sigma	
Software and Algorithms		
Adobe Suite CS6: Photoshop and Illustrator	Adobe	
ImageJ/Fiji		https://fiji.sc/
AxioVision 4.6	Zeiss	
Zen 2012 Blue edition	Zeiss	https://www.zeiss.com
Statistical R-Gui		https://www.r-project.org/
Other		
Pkd2-MO: 5' GGTGGATTCTGCTGGGATTCATCG 3'	Gene Tools, Philomath, USA	(Tran et al., 2010)
Xnr3-MO: 5' TCTCTGGGTAGATTTGTGGTGACTC 3'	Gene Tools, Philomath, USA	
Nodal1-MO: 5' GCTGTCAGAAATGCCATGCTTGAC 3'	Gene Tools, Philomath, USA	(Vonica and Brivanlou, 2007)
Dand5-MO1: 5' CTGGTGGCCTGGAACAACAGCATGT 3'	Gene Tools, Philomath, USA	(Vonica and Brivanlou, 2007)
Dand5-MO2: 5' TGGTGGCCTGGAACAACAGCATGTC 3'	Gene Tools, Philomath, USA	(Vonica and Brivanlou, 2007)
standard control-MO	Gene Tools, Philomath, USA	
Axioplan2 imaging microscope	Zeiss	
Zeiss LSM 700	Zeiss	
AxioCam HSm video camera	Zeiss	
Xenbase		https://xenbase.org
PubMed		https://www.ncbi.nlm.nih.gov/pubmed/

Supplemental References

- Belo, J.A., Bouwmeester, T., Leyns, L., Kertesz, N., Gallo, M., Follettie, M., De Robertis, E.M., 1997. Cerberus-like is a secreted factor with neutralizing activity expressed in the anterior primitive endoderm of the mouse gastrula. *Mechanisms of Development* 68, 45–57.
- Beyer, T., Danilchik, M., Thumberger, T., Vick, P., Tisler, M., Schneider, I., Bogusch, S., Andre, P., Ulmer, B., Walentek, P., Niesler, B., Blum, M., Schweickert, A., 2012. Serotonin Signaling Is Required for Wnt-Dependent GRP Specification and Leftward Flow in *Xenopus*. *Current Biology* 22, 33–39. doi:10.1016/j.cub.2011.11.027
- Blum, M., Beyer, T., Weber, T., Vick, P., Andre, P., Bitzer, E., Schweickert, A., 2009. *Xenopus*, an ideal model system to study vertebrate left-right asymmetry. *Dev. Dyn.* 238, 1215–1225. doi:10.1002/dvdy.21855
- Sbalzarini, I.F., Koumoutsakos, P., 2005. Feature point tracking and trajectory analysis for video imaging in cell biology. *J. Struct. Biol.* 151, 182–195. doi:10.1016/j.jsb.2005.06.002
- Sive, H.L., Grainger, R.M., Harland, R.M., 2000. *Early Development of Xenopus Laevis*. CSHL Press.
- Tran, U., Zakin, L., Schweickert, A., Agrawal, R., Doger, R., Blum, M., De Robertis, E.M., Wessely, O., 2010. The RNA-binding protein bicaudal C regulates polycystin 2 in the kidney by antagonizing miR-17 activity 137, 1107–1116. doi:10.1242/dev.046045
- Vick, P., Schweickert, A., Weber, T., Eberhardt, M., Mencl, S., Shcherbakov, D., Beyer, T., Blum, M., 2009. Flow on the right side of the gastrocoel roof plate is dispensable for symmetry breakage in the frog *Xenopus laevis*. *Developmental Biology* 331, 281–291. doi:10.1016/j.ydbio.2009.05.547
- Vonica, A., Brivanlou, A.H., 2007. The left–right axis is regulated by the interplay of *Coco*, *Xnr1* and *derrière* in *Xenopus* embryos. *Developmental Biology* 303, 281–294. doi:10.1016/j.ydbio.2006.09.039